Progress in Oceanography 88 (2011) 116–130

Contents lists available at ScienceDirect

Progress in Oceanography

journal homepage: www.elsevier.com/locate/pocean

Observed circulation in the Solomon Sea from SADCP data

Sophie Cravatte [a,b,*], Alexandre Ganachaud [a,c], Quoc-Phi Duong [d], William S. Kessler [e], Gérard Eldin [a,c], Pierre Dutrieux [f]

[a] Université de Toulouse, UPS (OMP-PCA), LEGOS, 14 Avenue Edouard Belin, F-31400 Toulouse, France
[b] IRD (Institut de Recherche pour le Développement), LEGOS, F-31400 Toulouse, France
[c] IRD, Nouméa, New Caledonia
[d] Ecole Nationale de la Météorologie, Toulouse, France
[e] PMEL/NOAA (Pacific Marine Environmental Laboratory/National Oceanographic and Atmospheric Administration)[1], Seattle, WA, United States
[f] British Antarctic Survey, Natural Environment Research Council, Cambridge, United Kingdom

ARTICLE INFO

Article history:
Received 25 June 2010
Received in revised form 9 December 2010
Accepted 19 December 2010
Available online 28 December 2010

ABSTRACT

The Solomon Sea, in the western tropical Pacific, is part of a major oceanic pathway for waters connecting the tropics to the equator via low latitude western boundary currents. Shipboard Acoustic Doppler Current Profiler data from 94 various cruises and transits are used to describe the Solomon Sea mean circulation and its seasonal variability above 300 m depth, providing an unprecedently detailed picture from observations. The circulation in the near-surface (20–100 m) and thermocline (100–300 m) layers were analyzed separately but found to have many similar features. They are compared with circulations inferred from hydrological and satellite data.

The New Guinea Coastal Undercurrent enters the Solomon Sea east of the Louisiade Archipelago (15 Sv inflow above 300 m), splits and rejoins around the Woodlark Chain, then divides against the coast of New Britain forming two branches flowing westward and eastward. The westward branch has been previously observed flowing through Vitiaz Strait; in the present SADCP data this transport is found to be 7–8 Sv in the upper 300 m. The eastward branch has been suspected and occurs in some models; it exits the Solomon Sea through St. George's Channel (1–2 Sv) and Solomon Strait (4–5 Sv) in the thermocline. At the surface, waters enter the Solomon Strait from the north.

The seasonal variability can be documented in locations of sufficient data coverage. It is shown that this western boundary system strengthens in June–August. A summary of transport variability in the straits of the Solomon Sea from individual cruises is also presented. Transports in the straits display some stable features, but also high non-seasonal variability.

1. Introduction

The Solomon Sea, in the western tropical Pacific north of the Coral Sea, is part of a major ocean circulation pathway. The low latitude western boundary currents (LLWBC) that cross this sea are an essential part of the subtropical cells that supply waters of mid to high latitude origin into the western equatorial Pacific (McCreary and Lu, 1994; Johnson and McPhaden, 1999; Schott et al., 2004). Some of these waters supply the Indonesian Throughflow, and some the equatorial current system (Lukas et al., 1996; Zenk et al., 2005). They notably contribute to the Equatorial Undercurrent (EUC), possibly to the southern subsurface countercurrent, and thereby feed the downstream surface waters of the cold tongue in the eastern Pacific (e.g., Tsuchiya, 1981; Tsuchiya et al., 1989; Fukumori et al., 2004). One of the main components of the LLWBCs in the area is the New Guinea Coastal Undercurrent (NGCU), flowing northwestward into the Solomon Sea and along the northern coast of Papua New Guinea (PNG).

At El Nino Southern Oscillation timescales (ENSO; 2–7 years), several modeling studies have suggested that the transports of the LLWBCs contribute as much as the interior route to the recharge/discharge of the equatorial warm water volume. Moreover, they have been shown to partially compensate the interior transport variability in ENSO (Lee and Fukumori, 2003; Hazeleger et al., 2004; Ishida et al., 2008; Schott et al., 2007). At decadal timescales, it has been suggested that changes in either the temperature (Gu and Philander, 1997; Giese et al., 2002; Yeager and Large, 2004; Luo et al., 2005) or the mass transport (Kleeman et al., 1999; McPhaden and Zhang, 2002; Nonaka et al., 2002; Lohmann and Latif, 2005; Lübbecke et al., 2008) of the subtropical waters arriving at the equator may modify the intensity and/or properties of equatorial upwelling. As a consequence, LLWBCs may modulate the background sea surface temperature at the equator, and thus

* Corresponding author at: IRD, LEGOS, 14 Avenue Edouard Belin, F-31400 Toulouse, France. Tel.: +33 5 61 33 30 05; fax: +33 5 61 25 32 05.
E-mail address: sophie.cravatte@legos.obs-mip.fr (S. Cravatte).
[1] PMEL Contribution # 3563.

0079-6611/$ - see front matter © 2010 Elsevier Ltd. All rights reserved.
doi:10.1016/j.pocean.2010.12.015

the El Nino Southern Oscillation (ENSO) cycle at low frequency (Fedorov and Philander, 2000; Sun et al., 2004; Chang et al., 2006; Matei et al., 2008). The LLWBCs therefore represent an important component of the equatorial heat and mass budgets at interannual and decadal time scales, and their associated transports of mass, heat and micro-nutrients are believed to play an important role in the global climate system (e.g., Gordon et al., 1997; Mackey et al., 2002; Izumo, 2005).

Quantifying the mean transports and associated oceanic currents variability in the Solomon Sea at seasonal, interannual and decadal timescales is thus crucial to a diagnosis of Pacific climate, and is an essential component of the CLIVAR/SPICE program (Climate Variability and Predictability/Southwest PacIfic ocean circulation and Climate Experiment) (Ganachaud et al., 2008). However, this remains challenging. The circulation in the region is intricate, due to the complex bathymetry and the presence of numerous islands and narrow straits (Fig. 1). The mean circulation has been coarsely described by indirect estimation (geostrophic calculations or geographical patterns of water mass properties) (Tsuchiya, 1968; Tsuchiya et al., 1989; Fine et al., 1994). Such estimates are valuable, but cannot resolve the distinct pathways produced by the complex network of straits. Direct current measurements in these areas of strong currents are sparse, and long time series are nonexistent. Observations from scattered surveys (Butt and Lindstrom, 1994; Lindstrom et al., 1987, 1990) have provided instantaneous estimates of transports at specific locations for short periods. Current meters deployed over 14 months in the Vitiaz Strait suggest that the permanently northward flow is modulated at seasonal timescales (Murray et al., 1995). Sea level data from tide gauges (Ridgway et al., 1993) and from altimetry data (Melet et al., 2010b) also revealed substantial interannual variability of surface transport in relation with ENSO.

Numerical simulations provide interesting insights into the time variability and spatial scales of Solomon Sea circulation; this is useful given the low data resources. However, simulations must properly resolve the complex bathymetry and the narrow straits to be realistic, which requires high-resolution modeling with attentive depiction of the straits topography. Using a 1/12° resolution OGCM simulation, Melet et al. (2010a) described the detailed mean and annual thermocline circulation in the Solomon Sea for the first time. They carefully adapted the model bathymetry to give a realistic representation of Solomon Sea straits. Indeed, they showed that the modeled transports are very sensitive to the bathymetry of the model. For example, modifying Vitiaz Strait width by 15 km (challenging for a model, yet about 30% of the total width) strongly impacts the transports. Velocity data and transport estimates are thus crucial to evaluate the realism of numerical simulations.

Perhaps the most widespread source of oceanic current data in the Solomon Sea comes from direct Shipboard Acoustic Doppler Current Profilers (SADCP) measurements. Most research vessels are equipped with SADCPs so that oceanic currents are recorded during either transits or research cruises. Most of these data have never been analyzed, or at least never put together to provide a comprehensive description of the oceanic circulation inside the Solomon Sea. The purpose of this study is to take advantage of historical SADCP measurements to describe the observed mean and annual cycle of surface and thermocline circulation in the Solomon Sea. It also aims at inferring the range of transport variations as well as the current structures and vertical extent in the straits. It will finally provide a useful database for numerical model validation.

This paper is organized as follows. Section 2 presents the data sources and the methodology used to construct a gridded monthly field of surface and thermocline currents. Section 3 describes the mean circulation obtained from these data. Section 4 estimates seasonal and interannual variability of currents and transports flowing through the straits, and Section 5 discusses our results and concludes.

2. Data and methods used

2.1. Shipboard Acoustic Doppler Current Profiler data

2.1.1. Description and filtering

Since the 1980s, research, military and some commercial vessels have been equipped with hull-mounted Acoustic Doppler Current Profilers (ADCP). The ADCP provides estimates of the horizontal velocity components as a function of depth, based on the Doppler effect of sound wave reflections against small particles carried by ocean currents. Such velocity profiles are obtained approximately every second and averaged over several minutes (typically 5 min) and vertically every ~8 m (Hummon and Firing,

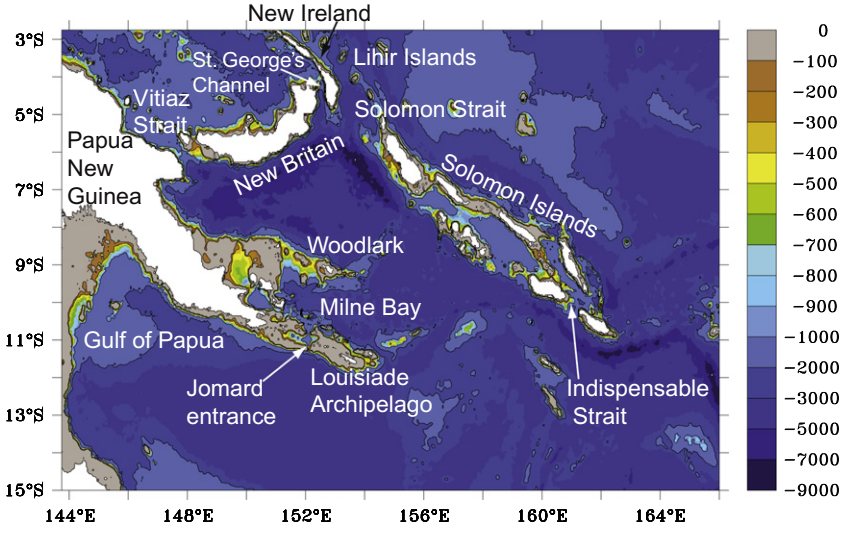

Fig. 1. Bathymetry of the Solomon Sea, in meters. The names of the main islands and straits are indicated. The Solomon Sea, in the center, is delimited to its east and its north by a quasi-continuous boundary formed by New Britain and the Solomon Islands. This boundary is interrupted by the narrow passages of Vitiaz Strait, St. George's Channel, Solomon Strait and Indispensable Strait. To its south, the Solomon Sea presents a wide opening to the Coral Sea.

Table 1
Cruise list and data sources. Lindstrom90 corresponds to digitalized data from the Lindstrom et al. (1990) figures of averaged along-strait ADCP transport over several repeats. JASADCP = University of Hawaii Joint Archive for Shipboard ADCP (http://ilikai.soest.hawaii.edu/sadcp/index.html); MARLIN = CSIRO Marine Laboratories Information Network (http://www.marine.csiro.au/maru/marlin_admin.survey_list); IRD-SADCP = ADCP-Institut de Recherche pour le Developpement (http://www.ird.nc/ECOP/sadcp_inventory.html).

	Cruise	Start	End	Ship	Source	Programme
1	wepocs 85	25-Jun-1985	06-Jul-1985	*Th. Thompson*	JASADCP	WEPOCS
2	fr8507vt	24-Jul-1985	24-Jul-1985	*Franklin*	Lindstrom90	WEPOCS-Vitiaz
3	fr8507stg	01-Aug-1985	01-Aug-1985	*Franklin*	Lindstrom90	WEPOCS-St. Georges
4	mw8516	26-Nov-1985	28-Nov-1985	*Moana Wave*	JASADCP	
5	mw8517	30-Nov-1985	22-Dec-1985	*Moana Wave*	JASADCP	
6	mw8518	26-Dec-1985	05-Jan-1986	*Moana Wave*	JASADCP	
7	fr8601vt	10-Jan-1986	10-Jan-1986	*Franklin*	Lindstrom90	WEPOCS-St. Georges
8	mw8601	18-Jan-1986	31-Jan-1986	*Moana Wave*	JASADCP	WEPOCS-Vitiaz
9	fr8601stg	05-Feb-1986	05-Feb-1986	*Franklin*	Lindstrom90	WEPOCS-Vitiaz
10	xyh5 us-prc2	13-Dec-1986	17-Dec-1986	*X.Y. Hong 5*	JASADCP	
11	xyh14 us-prc3	19-Oct-1987	23-Oct-1987	*X.Y. Hong 14*	JASADCP	
12	fr8804	25-Apr-1988	23-May-1988	*Franklin*	MARLIN	
13	xyh14 us-prc4	21-May-1988	25-May-1988	*X.Y. Hong 14*	JASADCP	
14	fr8805	25-Jun-1988	15-Jul-1988	*Franklin*	MARLIN	
15	xyh14 us-prc5	15-Nov-1988	18-Nov-1988	*X.Y. Hong 14*	JASADCP	
16	xyh14 us-prc6	21-May-1989	24-May-1989	*X.Y. Hong 14*	JASADCP	
17	xyh14 us-prc7	18-Nov-1989	22-Nov-1989	*X.Y. Hong 14*	JASADCP	
18	xyh14 us-prc8	18-Jun-1990	27-Jun-1990	*X.Y. Hong 14*	JASADCP	
19	fr9006	07-Jul-1990	25-Jul-1990	*Franklin*	MARLIN	
20	fr9007	07-Sep-1990	30-Sep-1990	*Franklin*	MARLIN	
21	fr9008a	01-Oct-1990	02-Oct-1990	*Franklin*	MARLIN	
22	fr9008b	10-Oct-1990	15-Oct-1990	*Franklin*	MARLIN	
23	alize2	01-Mar-1991	04-Mar-1991	*Le Noroit*	IRD-SADCP	
24	su0014	13-Mar-1991	05-Apr-1991	*Le Noroit*	IRD-SADCP	
25	fr9106	13-Jul-1991	29-Jul-1991	*Franklin*	MARLIN	
26	su0015	20-Jul-1991	12-Aug-1991	*Le Noroit*	IRD-SADCP	
27	coare1	22-Aug-1991	13-Sep-1991	*Le Noroit*	IRD-SADCP	
28	su0016	21-Jan-1992	13-Feb-1992	*Le Noroit*	IRD-SADCP	
29	mw9203	18-Feb-1992	02-Mar-1992	*Moana Wave*	JASADCP	
30	coare2	23-Feb-1992	14-Mar-1992	*Le Noroit*	IRD-SADCP	
31	fr9205	17-Jun-1992	12-Jul-1992	*Franklin*	MARLIN	
32	fr9206	14-Jul-1992	02-Aug-1992	*Franklin*	JASADCP	
33	su0017	08-Aug-1992	30-Aug-1992	*Le Noroit*	IRD-SADCP	
34	coare3	07-Sep-1992	29-Sep-1992	*Le Noroit*	IRD-SADCP	
35	kex1 leg1	10-Nov-1992	11-Dec-1992	*Kexue*	JASADCP	
36	xyh5 leg1	30-Nov-1992	01-Dec-1992	*X.Y. Hong 5*	JASADCP	
37	fr0992	19-Nov-1992	15-Dec-1992	*Franklin*	JASADCP	
38	xyh5 leg2	14-Dec-1992	15-Dec-1992	*X.Y. Hong 5*	JASADCP	
39	kex2 leg2	18-Dec-1992	23-Jan-1993	*Kexue*	JASADCP	
40	coare-poi	04-Dec-1992	26-Feb-1993	*Le Noroit*	JASADCP	
41	fr0193	08-Jan-1993	07-Feb-1993	*Franklin*	JASADCP	
42	sy3l3 leg3	28-Jan-1993	30-Jan-1993	*Shi Yan 3*	JASADCP	
43	kex3 leg3	31-Jan-1993	19-Feb-1993	*Kexue*	JASADCP	
44	mw9303	06-Apr-1993	18-Apr-1993	*Moana Wave*	JASADCP	
45	mw9304	21-Apr-1993	23-May-1993	*Moana Wave*	JASADCP	
46	fr9306 p11s	25-Jun-1993	30-Jun-1993	*Franklin*	JASADCP	
47	tn026	07-Oct-1993	13-Oct-1993	*Franklin*	JASADCP	
48	fr9308	09-Nov-1993	26-Nov-1993	*Franklin*	MARLIN	
49	flup75	24-Sep-1994	28-Sep-1994	*Atalante*	IRD-SADCP	
50	flu300	24-Sep-1994	28-Sep-1994	*Atalante*	IRD-SADCP	
51	k9406 leg 1	26-Dec-1994	28-Dec-1994	*Kaiyo*	JASADCP	
52	gp495 pr15	02-May-1995	03-May-1995	*Discoverer*	JASADCP	
53	nouz75	26-Feb-1996	29-Feb-1996	*Atalante*	IRD-SADCP	
54	nouz30	26-Feb-1996	29-Feb-1996	*Atalante*	IRD-SADCP	
55	kaon75	03-Jul-1996	07-Jul-1996	*Atalante*	IRD-SADCP	
56	ka9601	06-Jul-1996	09-Jul-1996	*Ka'imimoana*	JASADCP	
57	k9606 leg 1-2	25-Jul-1996	27-Jul-1996	*Kaiyo*	JASADCP	
58	fr9704	09-May-1997	22-May-1997	*Franklin*	MARLIN	
59	ka9702	15-Jun-1997	17-Jun-1997	*Ka'imimoana*	JASADCP	
60	fr9706	18-Jul-1997	02-Aug-1997	*Franklin*	MARLIN	
61	ky9709 leg 1-2	11-Aug-1997	12-Aug-1997	*Kaiyo*	JASADCP	
62	fr9707	04-Aug-1997	21-Aug-1997	*Franklin*	MARLIN	
63	ka9805	12-Jul-1998	14-Jul-1998	*Ka'imimoana*	JASADCP	
64	ky9810 leg 1-2	24-Aug-1998	25-Aug-1998	*Kaiyo*	JASADCP	
65	rb9904 nauru99	18-Jun-1999	22-Jun-1999	*Kaiyo*	JASADCP	
66	ka9905	12-Aug-1999	14-Aug-1999	*Ka'imimoana*	JASADCP	
67	wes00l	16-Oct-1999	20-Oct-1999	*Alis*	IRD-SADCP	
68	r200001	14-Jan-2000	02-Feb-2000	*Franklin*	MARLIN	
69	fr0002a	04-Feb-2000	07-Feb-2000	*Franklin*	MARLIN	
70	fr0002b	07-Feb-2000	12-Feb-2000	*Franklin*	MARLIN	
71	fr0002c	12-Feb-2000	14-Feb-2000	*Franklin*	MARLIN	

Table 1 (*continued*)

	Cruise	Start	End	Ship	Source	Programme
72	fr0002d	20-Feb-2000	21-Feb-2000	*Franklin*	MARLIN	
73	wes002	15-Apr-2000	19-Apr-2000	*Alis*	IRD-SADCP	
74	fr0003	14-Apr-2000	03-May-2000	*Franklin*	MARLIN	
75	fr0004	05-May-2000	20-May-2000	*Franklin*	MARLIN	
76	ka0006	24-Jul-2000	26-Jul-2000	*Ka'imimoana*	JASADCP	
77	ky0006 leg2-3	05-Sep-2000	06-Sep-2000	*Kaiyo*	JASADCP	
78	ka0009	21-Nov-2000	23-Nov-2000	*Ka'imimoana*	JASADCP	
79	fr000l	31-Mar-2001	23-Apr-2001	*Alis*	IRD-SADCP	FRONTALIS-1
80	fr0202	01-Mar-2002	24-Mar-2002	*Franklin*	MARLIN	
81	fr0203	26-Mar-2002	15-Apr-2002	*Franklin*	MARLIN	
82	fr0002	04-Apr-2004	26-Apr-2004	*Alis*	IRD-SADCP	FRONTALIS
83	ka0404	25-Jul-2004	27-Jul-2004	*Ka'imimoana*	JASADCP	
84	km0418nb	24-Oct-2004	10-Nov-2004	*Kilo Moana*	JASADCP	
85	km0419 os38nb	12-Nov-2004	18-Dec-2004	*Kilo Moana*	JASADCP	
86	ka0408	28-Nov-2004	30-Nov-2004	*Ka'imimoana*	JASADCP	
87	km0420nb	19-Dec-2004	22-Dec-2004	*Kilo Moana*	JASADCP	
88	fr03 legl	24-Apr-2005	28-Apr-2005	*Alis*	IRD-SADCP	FRONTALIS
89	fr03 leg2	13-May-2005	17-May-2005	*Alis*	IRD-SADCP	FRONTALIS
90	secal3	14-Jul-2005	20-Jul-2005	*Alis*	IRD-SADCP	SECALIS-3
91	ka0504	22-Jul-2005	24-Jul-2005	*Ka'imimoana*	JASADCP	
92	mgln06mv	21-Jul-2006	28-Aug-2006	*Melville*	M. Tivey, WHOI	
93	ironEUC2006	23-Sep-2006	01-Oct-2006	*Kilo Moana*	Slemons et al. (2010)	
94	flusec	16-Aug-2007	24-Aug-2007	*Alis*	IRD-SADCP	FLUSEC

2003a,b). We mostly used the measurements from 20 to 300 m, which is the nominal range of 150 KHz ADCP equipments. Few cruises used equipment that reached below 300 m.

We selected SADCP data from 94 cruises crossing the Solomon Sea (Table 1). These were provided by the Joint Archive for Shipboard ADCP at the University of Hawaii (46 relevant cruises), the MarLIN database of the CSIRO (Commonwealth Scientific and Industrial Research Organization, Australia), mainly holding SADCP measurements from the R/V Franklin (21 cruises), and SADCP data from IRD (Institut de Recherche pour le Développement) (21 cruises). We added SADCP data from 6 additional cruises (e.g., IronEUC2006, Slemons et al., 2010; Dutrieux et al., submitted for publication). During the WEPOCS cruises in 1985 and 1986 (Lindstrom et al., 1990), valuable SADCP measurements were obtained in Vitiaz Strait and St. George's Channel onboard R/V Franklin. Unfortunately, these data are no longer accessible, so we digitized Figs. 9 and 10 from Lindstrom et al. (1990) to obtain average, cross strait velocities from WEPOCS.

The ADCP profiles we started with were already treated with the standard CODAS (Common Ocean Data Access System) procedure (e.g., Hummon and Firing, 2003a,b). We further filtered each cruise individually according to the following procedure: (a) hourly averaging when not already done; (b) detection of velocities larger than 2.5 standard deviations from the 20 surrounding profiles in time at each depth; (c) detection of the vertical second derivative of velocities that are larger than seven times the standard deviation of the 20 surrounding profiles; (d) final visual identification of outliers over groups of 20 profiles. For each outlier detection (b)–(d) manual data removal was done only when judged necessary – depending on the surrounding profiles, location, and topography. The outlier detection limits were chosen heuristically, starting with various thresholds.

The seasonal distribution of ADCP profiles indicates very good sampling in Vitiaz Strait, St. George's Channel, and in the western part of Solomon Strait. It also indicates good sampling south of the Louisiade Archipelago, along 165°E and along 156°E north of the Solomon Islands (Fig. 2). We will see in Fig. 10 that these are indeed the locations where seasonal variability could be analyzed. However, sampling is sparse on the south coast of New Britain and on the east coast of the Solomon Islands, where significant currents are suspected to occur, and in other large oceanic areas.

2.1.2. Tides and internal waves

As observed during cruises that held a fixed position for several days, diurnal and semidiurnal tidal amplitudes may reach 20–30 cm s^{-1} or more (not shown), and may cause aliasing in SADCP data. The available global barotropic tidal models (e.g., TPX06.2, FES2004 (Lyard et al., 2006)) have too coarse a resolution to correctly resolve the tides in the Solomon Sea, especially in the narrow straits, and modeled tidal velocity amplitudes are underestimated. In any case, the observed signal in the region is associated with baroclinic internal waves originating from interactions between barotropic tides and bathymetry (Gourdeau, 1998; Lyard and Le Provost, 2002). We believe that the optimal interpolation method used to grid the SADCP data is able to filter the tides in most of the regions (see Section 2.2).

The only locations where a careful tidal analysis could be done are Vitiaz Strait and St. George's Channel, where moorings have been previously deployed (Lindstrom et al., 1990; Murray et al., 1995). In Vitiaz Strait, 35 current meter records from five moorings deployed from February or July 1992 to April 1993 were decomposed into their major tidal constituents using classical harmonic analysis. The amplitude and phases of the dominant semidiurnal and diurnal tides (M2, O1 and K1) are found similar for each current meter, except at the surface and at the easternmost mooring located near a shallow reef. Based on these harmonics, a tidal hindcast is performed to correct the SADCP data in Vitiaz Strait. The same method is applied for the moorings deployed in St. George's Channel during WEPOCS, in 1985 and 1986. It is worth noting that the transports in the straits computed for each individual cruise with and without tidal corrections are very similar, with one exception in St. George's Channel in May 1988 (see Section 4.2). So, even during single cruises, SADCP sampling is able to filter the tides. This reinforces our conviction that tides will not be a major issue for our study.

2.1.3. Method of averaging in the straits

In Vitiaz Strait, St. George's Channel, Solomon Strait and south of Rossel Island (the easternmost island of the Louisiade Archipelago), an "average" velocity section (see Section 4) is calculated from the various SADCP in the following way. A reference section is defined so that it is close to major cross-strait cruises (e.g., WEPOCS). Along this section, velocities are averaged over horizontal

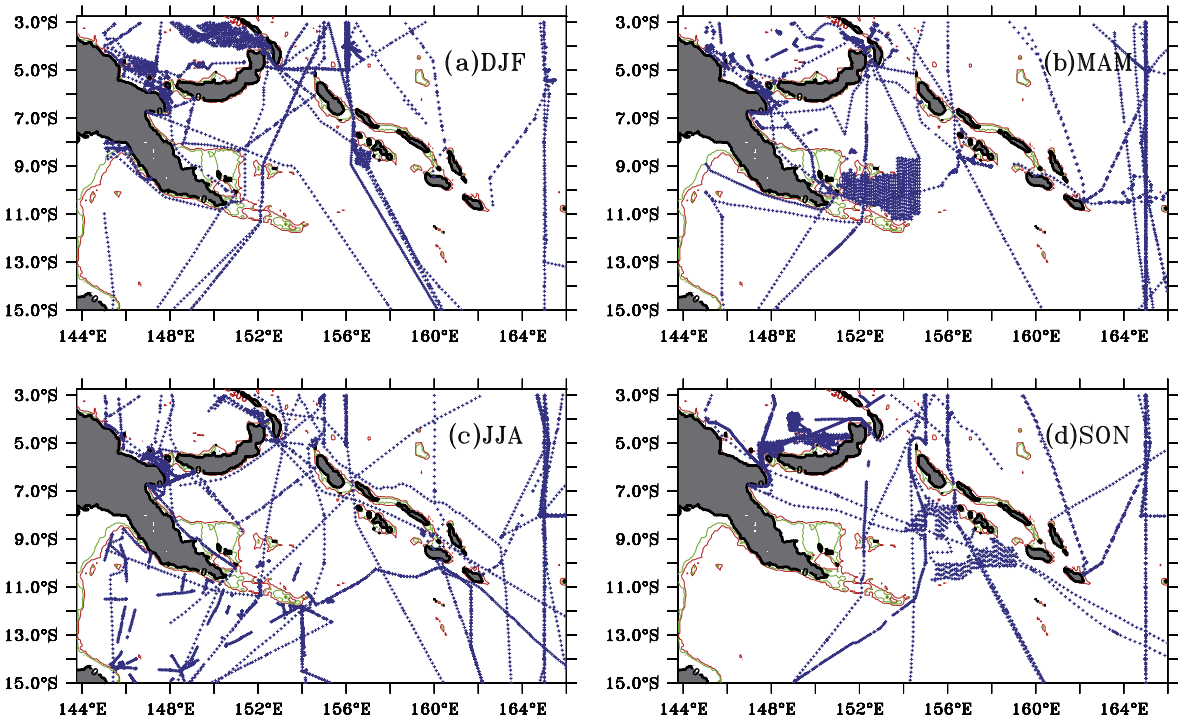

Fig. 2. Availability of SADCP data by seasons, after the data have been treated as described in Section 2.1.1. The green contour represents the 100 m isobath, and the red contour the 300 m isobath. (a) December, January, February; (b) March, April, May; (c) June, July, August; (d) September, October, November. (For interpretation of the references to color in this figure legend, the reader is referred to the web version of this article.)

bins whose resolution is chosen to optimize the averaging, based on the topography and data resolution. For each bin of the section, SADCP profiles are selected within a rectangular area whose length (in the cross section direction) is about five times the section bin width. Velocities from the selected SADCP profiles are then averaged for each bin to provide cross-strait average velocities.

2.2. Optimal Interpolation method

To estimate the circulation from SADCP data, which typically extends to 300 m, we define two depth ranges: the surface layer (20–100 m depth), under the direct influence of the wind stress, and what we call the "thermocline" layer (100–300 m depth), in which the major part of the NGCU core has been observed and is thought to be located (Lindstrom et al., 1987; Butt and Lindstrom, 1994; Qu and Lindstrom, 2002; Ueki et al., 2003; Melet et al., 2010a). This "thermocline" layer encompasses the isopycnal surfaces from 23.0 to 26.5 (based on the CARS climatology (see Section 2.3), not shown), and includes the 25.0 isopycnal characterizing the core of the EUC. SADCP data were first depth averaged in each layer and then mapped on a regular 0.25 by 0.25 degree longitude–latitude monthly grid using the three-dimensional (longitude, latitude and time) optimal interpolation method (OI) of De Mey and Ménard (1989). We separately mapped zonal and meridional components in each layer.

The optimal interpolation (OI) method provides an optimal value of the components of the current at each grid point (x, y, t) using only nearby data. A first guess field is obtained by gridding all the SADCP data using the OI with large correlation scales (50 km, 185 days). The differences between this first guess and the data are then mapped again using the OI method with smaller correlation scales. Small spatial correlation scales and relatively large time correlation scales (25 km and 61 days), were chosen to avoid excessive smoothing of the small spatial structures. We chose a large noise/signal ratio of 2 for the OI. This parameter is an estimate of the ratio of the variance of the noise to the variance of the process of interest. In our case, it represents all the variability that is not seasonal, which primarily is due to intraseasonal and interannual variability.

In addition to the interpolated current, the OI method provides an error estimate at each grid point (comprised between 0 and 1), which is given as a percentage of the variance of the signal represented. It depends mostly onto the number of available surrounding data. In our analysis, only interpolated fields with an error estimate of less than 80% of the variance of the signal represented will be taken into account.

Fig. 3 shows the number of SADCP profiles taken into account for each grid point, within a 25 km distance corresponding to the correlation radius. The region where our optimally interpolated currents are based on less than six profiles is shaded in grey. With sufficiently repeated profiles, the OI can filter the tides, if those are taken at different tidal phases. Because the effect of tidal aliasing is not possible to evaluate except in the specific cases discussed above given the dataset, we use a threshold of 12 as a crude indicator of vulnerability to aliasing of tidal currents. Some regions are very well sampled, with more than 1000 hourly profiles.

The SADCP gridded product, as well as the database of all hourly SADCP profiles, will be made available from the SPICE data page (http://www.ird.nc/UR65/SPICE/spice.html).

2.3. Other data

2.3.1. CARS 2009

To obtain an independent depiction of the mean surface and thermocline geostrophic currents in the Solomon Sea, we use the 2009 version of the CSIRO Atlas of the Regional Seas (CARS2009) (Ridgway et al., 2002; Condie and Dunn, 2006). CARS is an atlas of the mean, annual and semiannual harmonics of the ocean temperatures and salinities, allowing us to compute associated geostrophic velocities. The CARS atlas is provided on a 0.5 by 0.5

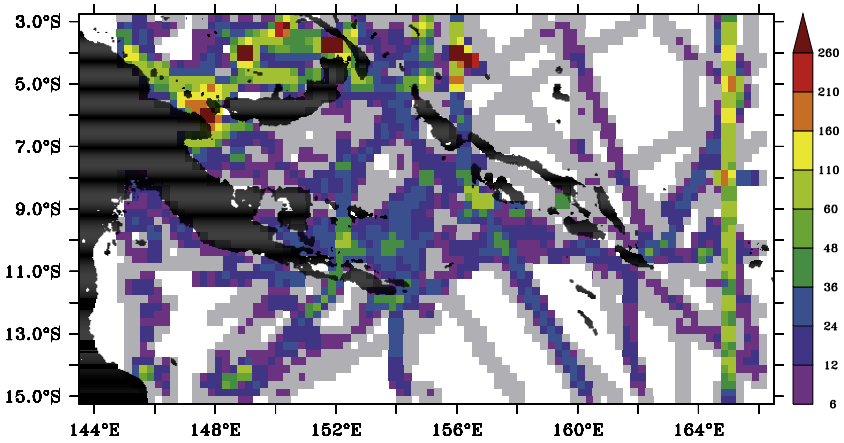

Fig. 3. Number of SADCP profiles in the ellipsoid of correlation (25 km radius) of each grid point of the OI, independently of time radius. The grey color is for numbers between 1 and 6. To emphasize the extensive shallow reefs, dark shading includes all regions above the 100 m isobath.

degree grid and standard depths. Because of the scarcity of data, the seasonal variability inferred from CARS appears to be unrealistic in this region (not shown), presumably because of the low data coverage, and will not be considered here. To compute the mean geostrophic currents, we chose a reference level of 1000 m, because a deeper reference level would result in losing too much information in shallow areas of the Solomon Sea. Some currents in this region, especially the NGCU at the entrance of the Solomon Sea, extend down to at least 2000 m with 10–20 cm/s (Maes et al., 2009), so the magnitude of the geostrophic currents may be underestimated there.

2.3.2. Mean dynamic topography and absolute geostrophic velocities

To get another independent view of the mean geostrophic surface currents, we use the absolute geostrophic surface currents computed from a modified version of the 1/4° Combined Mean Dynamic Topography (CMDT: CNES-CLS09). The original product is obtained by combining altimetric (GRACE, TOPEX/Poseidon, ERS 1/2) and in situ measurements (buoy velocities from which the ageostrophic component has been removed, XBT, and CTD casts in the 1993–2008 period). For a complete description, see Rio and Hernandez (2004), Rio et al. (2009). In the Rio et al. (2009) product, TOPEX and ERS1, 2 altimetric anomalies are subtracted from concurrent in situ measurements to obtain local estimates of the mean absolute dynamic topography. In our modified product, they are not, because subtracting altimetric anomalies may induce errors in coastal regions where the altimetric signals are not reliable.

3. Mean circulation in the Solomon Sea

Fig. 4 shows the mean circulation inferred from SADCP data, both in the surface (20–100 m) and in the thermocline layers (100–300 m) defined for the OI method. In contrast with what was expected from simulations (Melet et al., 2010b; Melet, 2010c), the estimated circulation is apparently not fundamentally different between surface and subsurface. Therefore we first describe the thermocline (100–300 m) circulation, of main interest because the LLWBCs have subsurface maxima, and then describe the differences with the surface (0–100 m) circulation. Transports computed from OI mean velocity fields are given indicatively in the text: they refer to the *total* transport above 300 m, therefore including surface and thermocline transports. The OI method does not constrain the flow to conserve mass, and does not allow accurate transports calculations. However, OI transports in the straits are very close to transports computed precisely from individual cruises (Section 4.2), and their summation eventually produces a nearly closed mass budget for the Solomon Sea.

3.1. Mean thermocline currents

The mean thermocline circulation in the Solomon Sea depicted in our analysis is intricate. Globally, it is consistent with previous studies (Fine et al., 1994; Melet et al., 2010a). The North Queensland Current (NQC) flows against the Great Barrier Reef of Australia and meanders clockwise in the Gulf of Papua until it becomes an eastward coastal current south of PNG (Fig. 4b). At this point Burrage (1993) and subsequent authors named it the "Hiri Current" (HC), referring to traditional trade routes used by Motu people of PNG. It is probable that the Hiri Current is the prolongation of the NQC, and whether it deserves a different name is debatable. We chose to keep the original "Hiri current" name. The HC sharply turns northward around the eastern tip of the Louisiade Archipelago, where it becomes the New Guinea Coastal Undercurrent. Our results indicate that the Hiri Current is not permanently abutting the coast in the Gulf of Papua. It forms meanders before turning north to enter the Solomon Sea to feed the New Guinea Coastal Undercurrent, consistently with the numerical results of Melet et al. (2010a). Across 11°S, at the tip of the Louisiade Archipelago, the NGCU, reaching speeds of 60–80 cm/s, is confined west of 156°E (with a width of about 150 km). It transports about 15 Sv above 300 m, consistent with the Sokolov and Rintoul (2000) estimation. A source of South Equatorial Current (SEC) waters, the North Vanuatu Jet at 10–13°S, also joins the NGCU directly and enters the Solomon Sea (11.5°S, 157°E). East of 156°E, across 11°S, the northward flow is weaker (less than 10 cm/s) and can reverse. Therefore the transport entering the Solomon Sea outside of the western boundary current (integrated from 156°E to the eastern boundary) is almost zero.

Our analysis points to two additional small inflows into the Solomon Sea. A shallow inflow of Hiri Current waters occurs through a narrow passage located west of the Louisiade Archipelago, called Jomard entrance (Fig. 1). This passage is a main ship route through the Louisiades, not wider than 10 km, with a 280 m maximum depth, where tidal currents are known to be important (1.5–2 m/s on a nautical chart). A close examination of meridional currents from 10 cruises passing through this passage confirms significant semidiurnal tide amplitude, of around 40–60 cm/s (not shown). Instantaneous currents can thus be strong. However, the mean 20–300 m meridional velocity is found to be 20 cm/s, and the mean northward transport of 0.3 Sv remains negligible compared to the

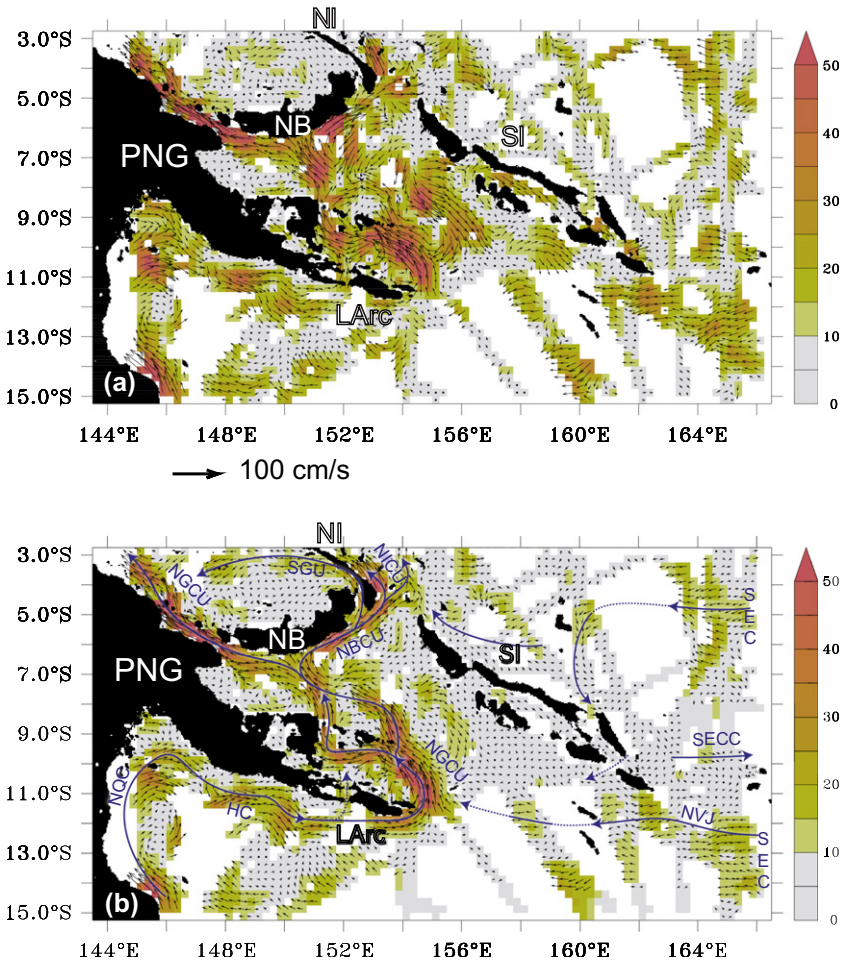

Fig. 4. Mean currents from the optimal interpolation analysis (OI): surface layer (20–100 m) (a) and thermocline layer (100–300 m) (b). Colors represent the mean velocity amplitude in cm/s. Grid points with no data are blanked. Abbreviations are: SI for Solomon Islands, NB for New Britain, NI for New Ireland, LArc for the Louisiade Archipelago and PNG for Papua New Guinea. Dark shading includes all regions above the 100 m isobath. Main currents are also schematically represented by the blue arrows. (For interpretation of the references to color in this figure legend, the reader is referred to the web version of this article.)

NGCU transport. To the east, in the deep, 50-km wide Indispensable Strait (Fig. 1), which is the only deep passage through the Solomon Islands chain, the OI velocities are weak (see the discussion Section 4.2).

Inside the Solomon Sea, the NGCU enters Milne Bay and splits around the Woodlark Islands. Then, the NGCU does not closely follow the New Guinea coast, but flows northward away from the boundary to the southern coast of the New Britain. This contrasts with the Melet et al. (2010a) numerical simulation, where the NGCU closely follows the New Guinea coast. Reaching New Britain, the NGCU here bifurcates around 7°S, 150°E, with one branch exiting through Vitiaz Strait, and the other branch flowing eastward along the southern coast of the New Britain as the New Britain Coastal Undercurrent (NBCU), as suggested by Fine et al. (1994) and modeled by Melet et al. (2010a). This current reaches speeds of more than 40 cm/s, and is confined within 1° of the coast. Elsewhere in the Solomon Sea, the thermocline circulation that can be measured here is characterized by eddies and recirculation.

At the northern boundary of the Solomon Sea, water exits toward the equator through three passages: Vitiaz Strait (45 km wide, 1200 m deep), St. George's Channel (30 km wide, 1100 m deep) and Solomon Strait (170 km wide, 4000 m deep). Water exiting northward from Vitiaz Strait forms a strong current with a mean core velocity of 80 cm/s, which transports about 7.5 Sv above 300 m. This feed a previously observed northwestward branch along the New Guinea coast (Cresswell, 2000; Kashino et al., 2007; Kuroda, 2000; Ueki et al., 2003). Water exiting St. George's Channel forms the St. George's Undercurrent (SGU, Lindstrom et al., 1990). It reaches 20–30 cm/s, and carries about 1.5 Sv; turns into the Bismarck Sea and potentially joins the NGCU. Water exiting through Solomon Strait (30–40 cm/s, about 5.5 Sv) feeds the New Ireland Coastal Undercurrent (NICU) along the east coast of New Ireland, as previously described by Butt and Lindstrom (1994) and Dutrieux et al. (submitted for publication). The NICU is divided by the Lihir Island chain, about 60 km offshore of New Ireland (Fig. 1), and its offshore branch could directly join the equatorial band.

East of the Solomon Island chain, numerical simulations suggest that the SEC feeds a northward western boundary current (Kessler and Gourdeau, 2007; Melet et al., 2010a). This current may eventually enter the Solomon Sea through Solomon Strait or join the NICU. The Island rule theory predicts a net southward western boundary current (Qiu et al., 2009). SADCP observations here suggest a bifurcation of the SEC along the eastern coast of the Solomon Islands around 7°S, with flow equatorward north of the bifurcation and poleward south of it. Whether such a circulation is real or not would need to be confirmed by more focused measurements, as we have only data from 1 cruise between 156°E and 160°E, east of the quasi-continuous barrier formed by the Solomon Islands (Fig. 3).

Comparison of our analysis with CARS geostrophic currents (Fig. 5b) shows similar main circulation patterns. It corroborates the presence of meanders south of the Louisiade Archipelago, two branches feeding the NGCU at the entrance of the Solomon Sea (one from the Gulf of Papua and one directly from the SEC). Interestingly, CARS indicates a bifurcation east of the Solomon Island chain around 6°S. However, the scarcity of hydrological data in the Solomon Sea and the interpolation in CARS result in geostrophic current structures smoother than in the real ocean. The SADCP allow a much more detailed description of the waters pathways inside the Solomon Sea.

3.2. Mean surface currents

At the surface (Fig. 4a), the mean circulation is broadly similar to the thermocline circulation (Fig. 4b), with the following notable differences. In the western part of Solomon Strait, as well as in St. George's Channel, the mean northward flow is weaker in the surface layers by about 15–25 cm/s, and it can actually reverse, as we will see in Section 4.2. The mean surface flow is also significantly weaker by 15–20 cm/s east of the Louisiade Archipelago. Significant surface-layer southeastward flow is seen in the eastern Solomon Sea (velocities higher than 20 cm/s), and in New Georgia Sound between the two chains of the Solomon Islands (158°E, 8°S). It is worth noting that these observed surface flows are not in the direction of the Ekman currents (southwestward) computed with QuickSCAT wind stresses, which were found to be much smaller than the geostrophic currents and will not be discussed further here.

Similar but smoother features are seen in the CARS surface geostrophic currents (not shown). Absolute geostrophic surface circulation computed from the modified CMDT (Fig. 5a) is comparable to Fig. 4a, which represents the 20–100 m depth layer. (Given the different depth range between the two data sets, and the fact that CMDT only represents the geostrophic currents, the comparison remains qualitative. However, Ekman transports are negligible.) Interestingly, this independent dataset confirms, owing mostly to the inclusion of in situ drifter data (M.-H. Rio, personal communication), the mean schematic surface circulation in the Solomon Sea. It confirms the bifurcation of the New Guinea Coastal Current around the Woodlark Islands, its bifurcation at the coast of New Britain, the presence of an eastward current confined along the New Britain coast, southward flow inside the Solomon Sea and inside the Solomon Islands chain. As in the CARS product, it indicates a bifurcation of the SEC near 7°S east of the Solomon Islands chain. Theses patterns are very similar to the near-surface currents 1° climatology obtained from drifters only (Lumpkin and Garraffo, 2005).

In contrast with our estimate, CMDT shows a strong entering flow through Solomon Strait, that partially crosses the Solomon Sea westward and exits through Vitiaz Strait and that could partially turn east and join the New Guinea Coastal Current, or exit through the southern entrance of the Sea, consistent with the modeled surface circulation from Melet et al., 2010b (their Fig. 1b).

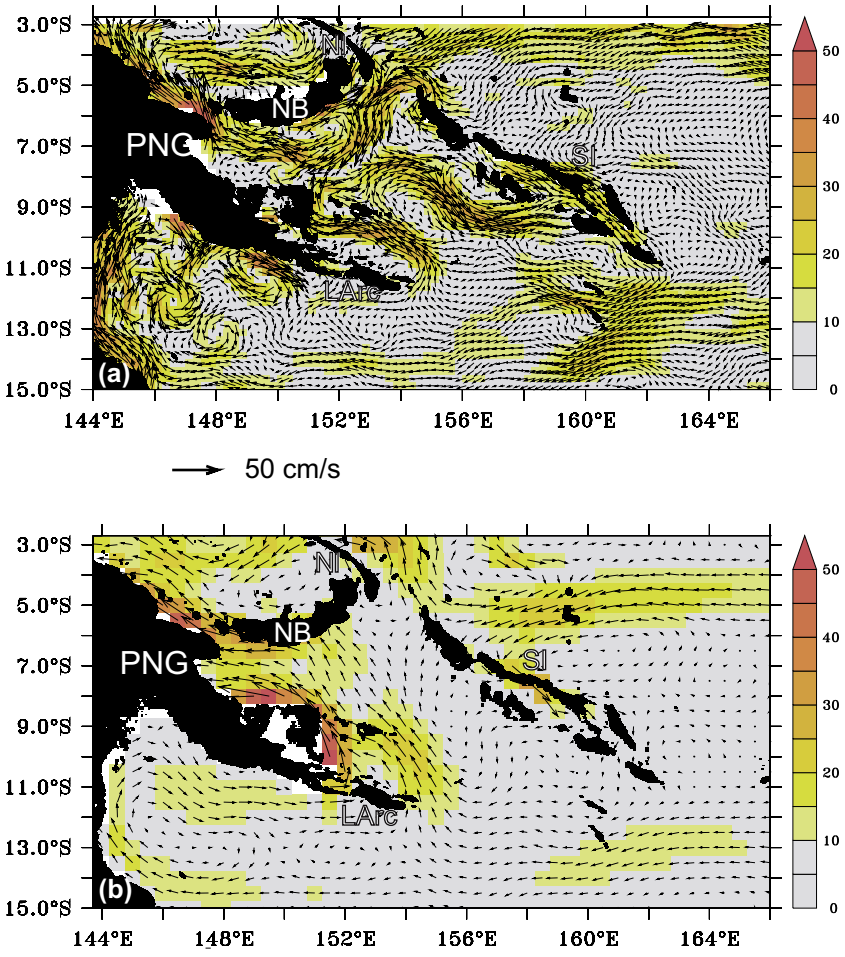

Fig. 5. Same as Fig. 4 but for different products. (a) Absolute surface geostrophic currents from a modified version of CMDT (Combined Mean Dynamic Topography) product. (b) CARS2009 thermocline geostrophic currents relative to 1000 m, averaged from 100 to 300 m depth.

Whether the differences are due to a surface flow that is different to that of our upper layer average is not clear.

3.3. Details in key regions

In previous sections, we examined the mean circulation vertically averaged in two layers. We now examine the current depth, position and variability in key, well-sampled regions: Vitiaz Strait, St. George's Channel, Solomon Strait, and south of the Louisiade Archipelago. The straits are the bottlenecks by which waters exit the Solomon Sea, and the section south of the Louisiades spans the western boundary current pathway.

3.3.1. Vitiaz Strait

In total, 15 cruises sampled entirely Vitiaz Strait, but only four of these extended below 300 m depth. Fig. 6 shows the mean current and its standard deviation from all cruises (see Section 2.1.3). During many of the cruises the NGCU had a clear subsurface maximum, which is somehow blurred in the mean because of occasional cases of surface maxima. Its core is located on the western half of the strait (in all cruises but one) around 150–300 m, and with typical speeds of 70–90 cm/s (occasionally reaching 120 cm/s). The NGCU extends deep, and velocities as high as 50 cm/s are still observed at 500 m depth, confirming the Lindstrom et al. (1990) observations. Whereas the NGCU is stable at its core depth (standard deviation is less than 20 cm/s), its standard deviation is largest within the first 50 m, where it reaches 40 cm/s. During the southeasterly monsoon in austral winter, the surface northwestward current is maximum, often greater than the subsurface current, as observed by Murray et al. (1995). During the northwesterly monsoon in austral summer, the surface northwestward current is minimum and may even reverse to become southeastward, explaining the large standard deviation in the surface layer.

3.3.2. St. George's Channel

At the entrance of St. George's Channel (Fig. 7a), the core of the SGU subsurface current is located at a depth around 200–300 m, with velocities around 30 cm/s, mostly located in the eastern part of the channel. When passing Duke of York Island, located at 4.20°, 152.45°, in the middle of the channel exit (Fig. 7b), it splits into two branches, one shallower, to the west of the island, and another deeper and stronger (40–50 cm/s) to the east. However, tides and internal waves are found to be important (several tens of cm/s) in the channel, as revealed by our analysis of WEPOCS moorings (Section 2.1.2). The variability seen in Fig. 7 is high and comparable to the mean current, in both surface and subsurface. An examination of individual sections reveals that surface currents occasionally reverse, and that the consistent northward cores in the thermocline varies both in position and strength.

3.3.3. Solomon Strait

Only 5 cruises cross the wide Solomon Strait entirely. However, the subsurface horizontal structures of the currents are very similar in these cruises, suggesting a robust signal. Averaged SADCP data indicates a northward undercurrent with velocities of 30–50 cm/s, located around 150–300 m depth on the western side of the strait (Fig. 8). In the eastern part of the strait, the subsurface current is southward (10–15 cm/s), and close to the eastern boundary, it is weakly northward. In the surface layer, currents are highly variable, with alternating entering and exiting flow, and mean southward currents (18 cm/s) lower than the standard deviation (30 cm/s rms). This compilation of selected cruises results in a flow that contrasts with that of the OI, which indicated a mean

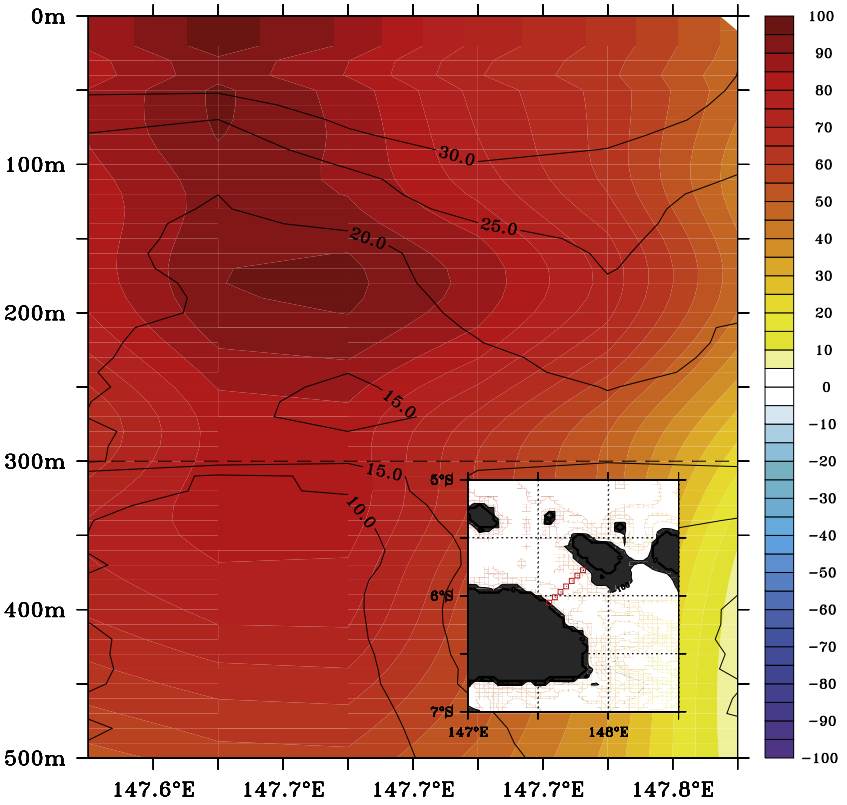

Fig. 6. Mean cross section velocities (colors) and standard deviation (contours) across Vitiaz Strait from 15 cruises along the red section in the inset (see text). Velocities are extrapolated from 20 m to the surface. Only 4 cruises have measurements below 300 m (dashed line). Along this section, velocities are averages over six 6.2-km bins (0.04° in longitude). Units are cm/s. (For interpretation of the references to color in this figure legend, the reader is referred to the web version of this article.)

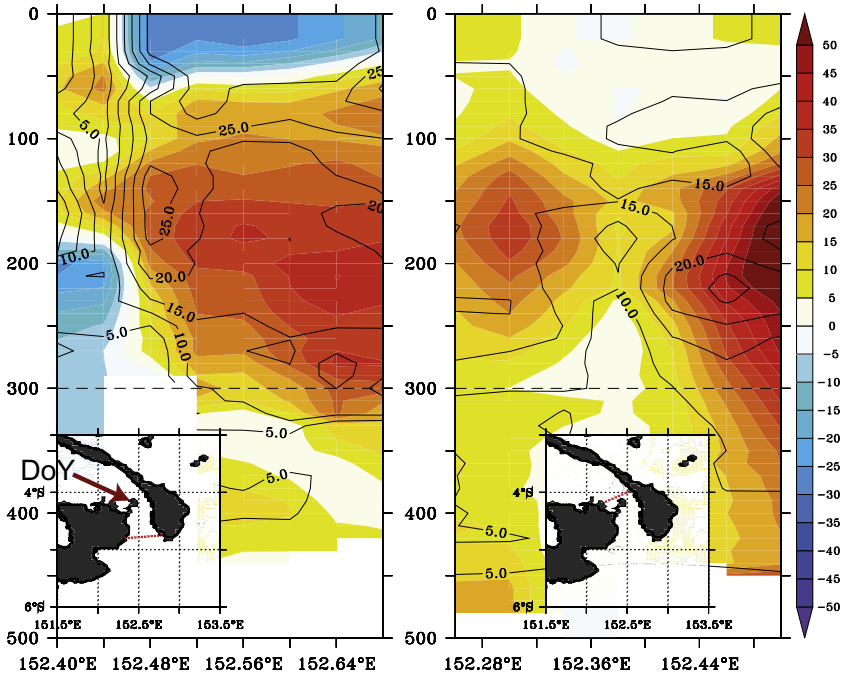

Fig. 7. Same as Fig. 6 but in St. George's Channel from 8 cruises (a) and 6 cruises (b). DoY indicates "Duke of York Island". Along these sections, velocities are averages over 8 bins of 4.4 km for the south projection section, 7 bins of 5.1 km for the north (0.04° in longitude). Only 1 cruise for the south section and 2 cruises for the north section have measurements below 300 m (dashed line). Velocities are extrapolated from 20 m to the surface. Units are cm/s.

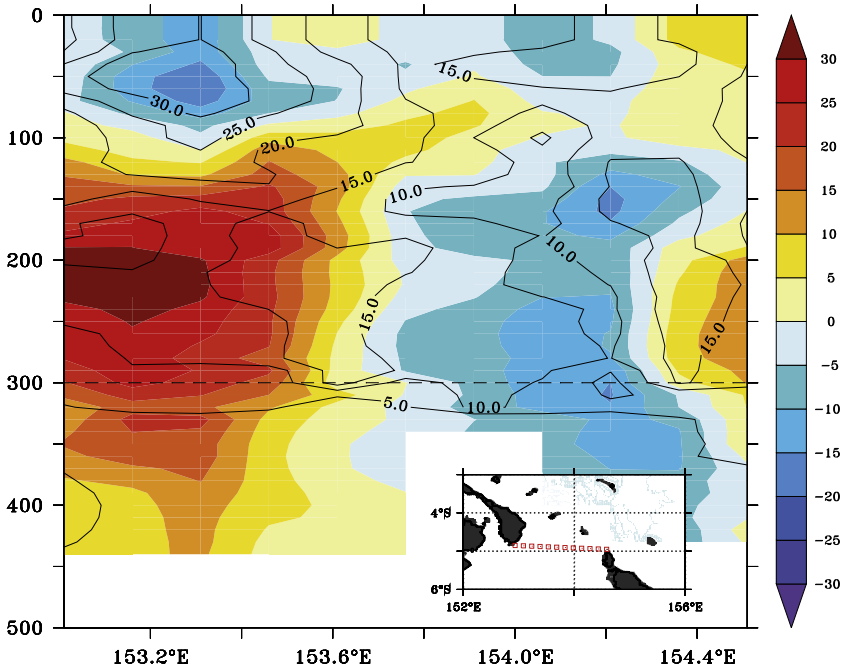

Fig. 8. Same as Fig. 6 but in Solomon Strait from 5 cruises. Along this section, velocities are averages over 11 bins of 16.6 km (0.15° in longitude). Only 1 cruise has measurements below 300 m (dashed line). Velocities are extrapolated from 20 m to the surface. Units are cm/s.

southward surface flow in the central and eastern part of the strait, but a mean northward surface flow in the western part of the strait (Fig. 4a). As seen in Fig. 3, the OI integrates many cruises that are not included in this 5 cruises average because they did not cross the entire strait, and thus uses many more vertical profiles. This sign difference is expectable given the high variability in the upper layer (Fig. 8), and points to the limitation of our dataset sampling.

An analysis of 49 surface drifters trajectories from the Global Drifter Program (Lumpkin and Pazos, 2006) crossing the Solomon Strait was performed. It indicates that 46 drifters drifted southwestward, 1 northeastward, 2 first westward then back eastward (not shown). Similarly, surface velocity from the CMDT product is southward (Fig. 5a), suggesting that the surface flow (at around 15 m depth) through Solomon Strait is much more often entering than exiting the Solomon Sea.

3.3.4. South of the Louisiade Archipelago

Finally, 7 cruises near the southern entrance of the Solomon Sea allow for a description of the upper vertical structure of the eastward Hiri Current before it turns north into the Solomon Sea. South of the Louisiade Archipelago at 154°E, the eastward boundary current keeps close to the coast, extending not further than 50–100 km offshore (Fig. 9). Farther than 150 km offshore, the flow reverses westward. This is consistent with the findings of Sokolov and Rintoul (2000). The vertical structure of the current is variable. The coastal 20–50 m surface current reverses in individual sections, flowing alternatively westward along the coast of New Guinea or eastward toward the entrance of Solomon Sea. The maximum zonal current (30–50 cm/s eastward) is subsurface, and often seen at the deepest observed level of individual cruises (200–300 m depth), suggesting that the NGCU core is near or deeper than 300 m. This is confirmed by glider (R. Davis, personal communication) and LADCP measurements (Maes et al., 2009), which identify the current core at 400–500 m depth. It thus appears that the NGCU core becomes shallower during its passage from the southern entrance to the northern exits of the Solomon Sea. Understanding why and how this occurs is an interesting question, but is beyond the scope of this study.

4. Variability

4.1. Seasonal variability

An understanding of seasonal variations from SADCP data is necessarily confined to locations with sufficient data availability. At locations sampled at least once during each of the four different seasons (DJF, MAM, JJA, SON), we compute the annual harmonic amplitude and phase from the OI analysis. The annual cycle is qualitatively similar at the surface and in the thermocline. The former is strongest, but the thermocline variability is more relevant since currents have subsurface maxima. This thermocline annual variability is presented (Fig. 10), following the representation of Kessler and Gourdeau (2007). The annual signal is described using variance ellipses (Fig. 10a), with their major and minor axes showing velocity standard deviations after the ellipse has been rotated to express the maximum possible variance in the direction of the major axis. The amplitude and phase of the major axis velocity component are presented in Fig. 10b as vectors, the size of the arrow representing the amplitude and its color the month of annual maximum current in the direction of the arrow. Each vector could be reversed with a corresponding phase change of 6 months.

It readily appears that the seasonal variability is often strongest in the direction of the mean currents (Fig. 10a), indicating that main variability is in amplitude rather than in direction. Fig. 10b also shows places of inconsistent phases in adjacent grid points, possibly due to sampling limitations. In these locations, results shown in Fig. 10 should be taken with caution.

Nevertheless, in some locations detailed below, the signal is more robust. East of the Solomon Sea, the westward-flowing SEC at 165°E from 3°S to 7°S is strongest in May–June (roughly consistent with the observations from Johnson et al. (2002)), and the eastward-flowing South Equatorial CounterCurrent (SECC) (8–12°S) is weaker in October–November (or equivalently stronger in April–May), in agreement with previous altimetric observations and Rossby wave models that indicate a maximum SECC in March, April, May (Chen and Qiu, 2004). The seasonal variability also appears as a very robust signal in Vitiaz Strait: the northwestward flow is stronger in JJA, during the southeasterly monsoon, and weaker in DJF, during the northwesterly monsoon. Currents are also stronger downstream along the New Guinea coast in August–September, in agreement with the ADCP data of the Japan Agency for Marine-Earth Science and Technology (JAMSTEC) subsurface mooring located at 142°E, 2.5°S (Kuroda, 2000; Ueki et al., 2003). In St. George's Channel, and downstream in the Bismarck Sea, the flow is stronger in May–June. In the western part of Solomon Strait, where the current is stronger, the maximum velocity is found in September–October–November.

Finally, at the wide southern entrance of the Solomon Sea, the northward current appears stronger in April–May–June south of

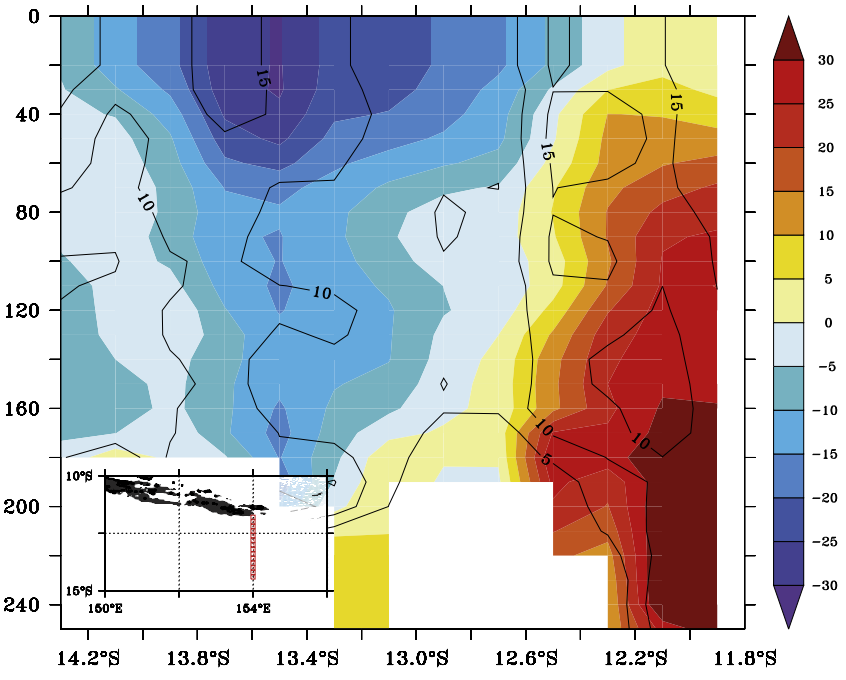

Fig. 9. Same as Fig. 6 but along 154°E south of the Louisiade Archipelago (7 cruises). Along this section, velocities are averages over 13 bins of 22 km (0.2° in latitude). Units are cm/s.

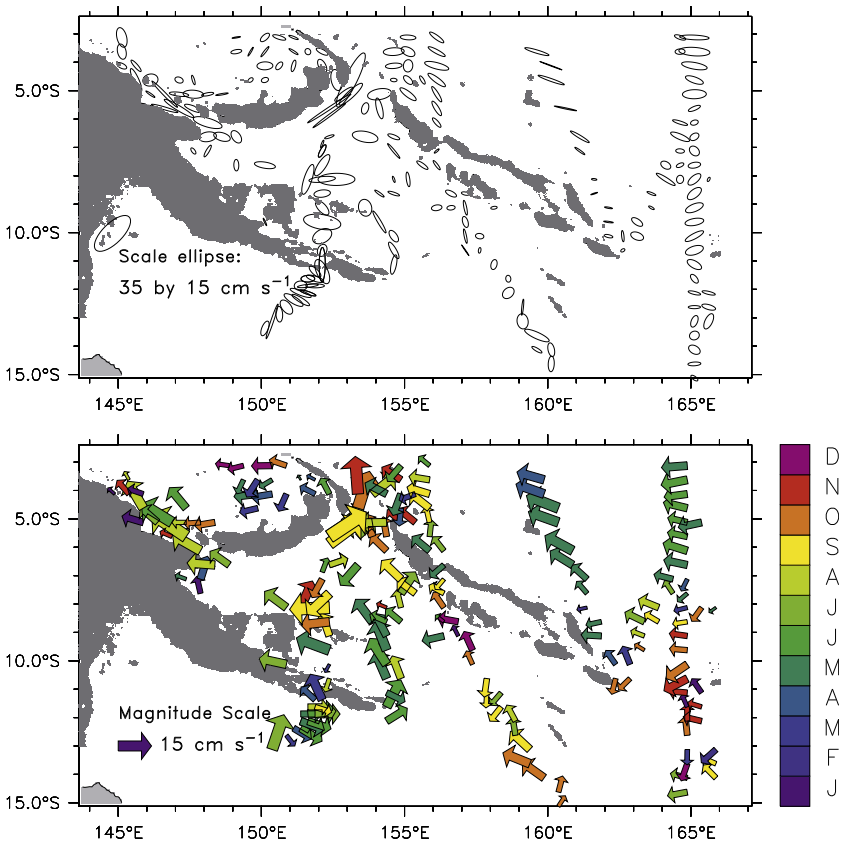

Fig. 10. Harmonic analysis from the thermocline (100–300 m) layer currents. Only the grid points where at least 4 months are sampled (one in each of the DJF, MAM, JJA, SON seasons) are considered. (Upper) Annual cycle variance ellipses (scale at lower left). (Lower) Annual cycle currents anomalies. The area of each vector indicates the magnitude of the 1-cpy harmonic (scale at lower left), the direction points along the major axes of the variance ellipses, and the color indicates the month of maximum current in the direction of the vector (scale at right). The choice of vector direction is arbitrary: each vector could be reversed, and its phase advanced by 6 months, to show the opposite phase of annual anomalies. (For interpretation of the references to colour in this figure legend, the reader is referred to the web version of this article.)

the Louisiade Archipelago, and stronger in June east of the Louisiade Archipelago.

Overall, all the LLWBCs, from the southern coast of the Louisiade Archipelago to north of Vitiaz and Solomon Strait, appear to strengthen from April to October, one or two months before and after the JJA strong southeasterly monsoon. These phase lags illustrate the complexity of the seasonal variability of circulation in the Solomon Sea.

The surface seasonal variability is not consistent at all with Ekman dynamics, that would force a seasonal reversal of the currents from northeastward in January/February to southwestward 6 months latter (not shown). Thus, seasonal variability of the circulation is largely geostrophic, which is consistent with the findings of Melet et al. (2010a,b). In their 1/12° model, these authors conclude that the seasonal variability of the thermocline currents in the Solomon Sea responds to the basinwide wind forcing that modulate incoming and outgoing transports. They also noted the complexity of the current's phasing, resulting from the combination of different dynamical forcing (equatorial dynamics, remotely forced Rossby waves, spin up and down of the subtropical gyre). Interestingly, our seasonal phasing is very consistent in most locations with the seasonal variability inferred from their high-resolution model (Fig. 6 of Melet et al., 2010a) and from altimetry (Melet et al., 2010b).

4.2. Water mass transport variability

Finally, we evaluate the range of transport variability in the upper layers of the Solomon Sea straits for the whole time range of our data set. Transports are calculated from selected individual cruises that had enough spatial coverage during a single cruise. Because they are based on coast-to-coast sections, we believe that they are more accurate than the ones calculated from products such as the OI or strait velocity averages. ADCP data are binned on a regular grid along the track line, and projected on cross-track and along-track components. Integration of cross-track component provides the transports.

The strait transports (Fig. 11) reveal significant variability, with strong interannual and/or intraseasonal transport variability in addition to the seasonal variations described in the previous section. It is not possible however, given the limited number of transport estimates, to discriminate between those scales of variability.

Transport through Vitiaz Strait over 13 cruises displays a range of 2.8–12 Sv in the 0–300 m layer (note that this is not the total transport; significant transport is also known to occur deeper: e.g., 6.0 Sv during the IronEUC2006 cruise of 2006 flowed below 300 m). Transport in the thermocline waters ranges from 3.6 to 7 Sv, with highest transports during JJA (6.1 Sv), in agreement with the SADCP velocities harmonic analysis. The transport is more variable in the upper layers (yellow bars on Fig. 11), with one occurrence of seasonal reversal (1 Sv) in January, during the northwesterly monsoon, while transport ranges from 1 to 5.4 Sv northward for the rest of the year, with maximum in JJA and SON (~4.2 Sv). In their high-resolution model, Melet et al. (2010a) found smaller variability on seasonal timescales but higher transports, ranging from 6.5 Sv (FMA) to 8 Sv (ASO). This difference may be partly due to their deeper layer definition (0–350 m), and the sensitivity of their result to the modeled strait width.

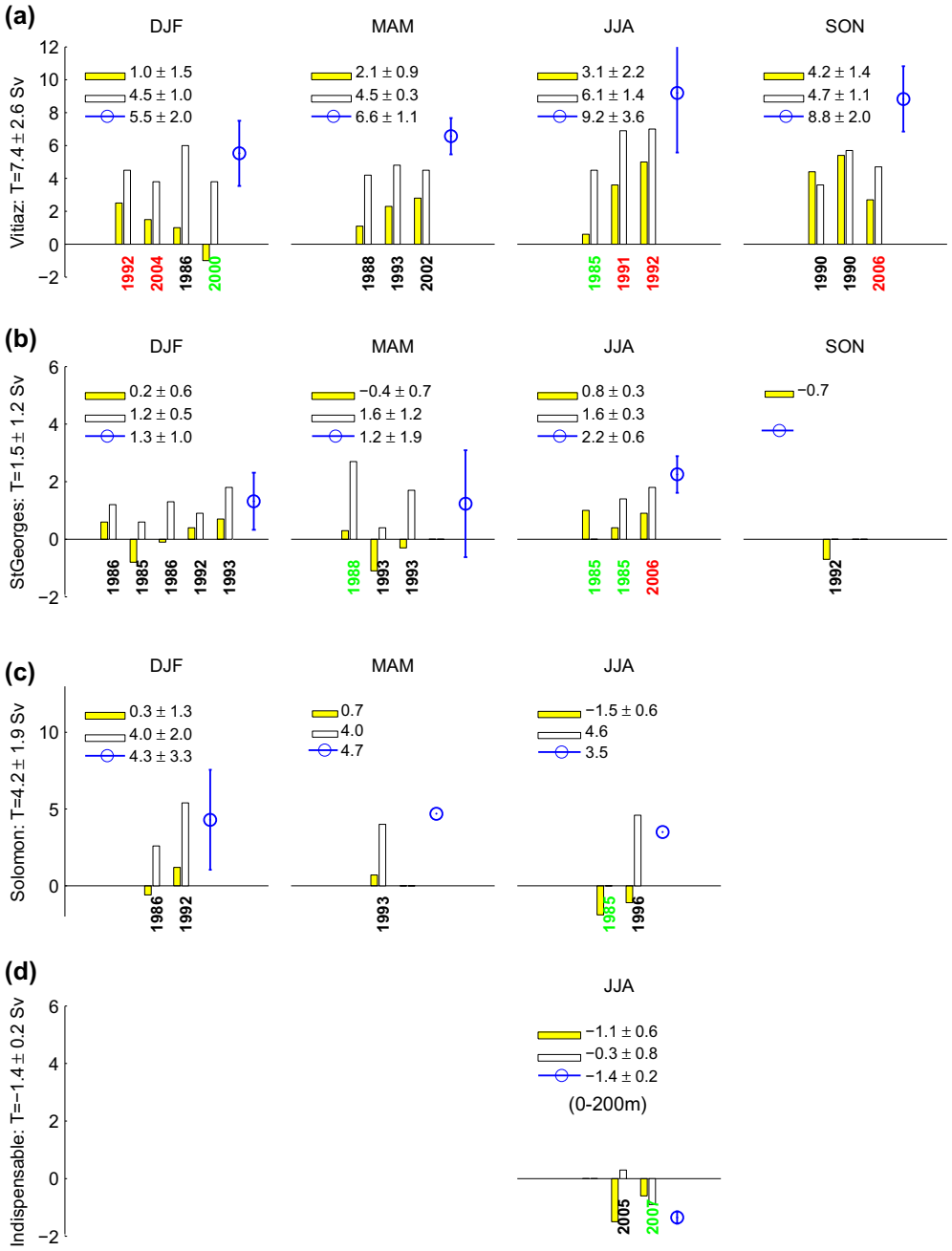

Fig. 11. Summary of transport estimates in the straits. The yellow bars indicate the upper (0–100 m) transport; the white bars represent the "thermocline" transport (100–300 m) through (a) Vitiaz Strait; (b) St. George's Channel; (c) Solomon Strait and (d) Indispensable Strait (only to 200 m). Transport estimates are given in Sv, for each cruise referenced by cruise year (label on *x*-axis) and grouped by season (each column; DJF, MAM, JJA and SON). For each graphic, the legend provides the seasonal average (e.g., $U = 2.4 \pm 0.2$) while the blue circle (error bar and legend) provides the total 0–300 m seasonal average. The annual average transport for each strait is provided by the vertical axis label on the left. The cruise years are color-coded according to the ENSO status during the cruise month: neutral situation (black); El Niño (red) and La Niña (green). (For interpretation of the references to color in this figure legend, the reader is referred to the web version of this article.)

The St. George's Channel thermocline transport estimates are smaller than in Vitiaz Strait. They range from 0.4 to 2.7 Sv northward. Surface transport is varying between −1 Sv and 1 Sv. The best documented season, DJF, suggests a strong non-seasonal variability, with mean thermocline transport of 1.2 ± 0.5 Sv to the north and 0.2 ± 0.6 Sv in the surface layer.

In Solomon Strait, thermocline transport was always measured northward, ranging from 2.6 to 5.4 Sv while surface transports ranged from 2 Sv southward to 1.2 Sv northward, confirming the high variability seen in Fig. 8. The transport variations mainly follow those of the western part of the strait, against the coast (not shown).

Indispensable Strait (50 km wide, 1600 m deep in some places), larger than Vitiaz Strait, is potentially another important gate for Solomon Sea waters. The 2 cruises that crossed it provide only limited information about the range of variation of the transport. This transport was weak and westward during the 2 cruises: 0.6 Sv and 1.5 Sv at the surface, and 1.2 Sv in the thermocline in 2007 (0–200 m).

Ridgway et al. (1993) and Melet et al. (2010b) reveal significant interannual variability of the strait transports in phase with El Nino. Ridgway et al. (1993), using sea level data, estimated that the transport through Vitiaz Strait increased by about 15 Sv during

the 1986–1987 El Nino event, and Melet et al. (2010b), from altimeter data, estimated a transport variation in both Vitiaz and Solomon Strait of about 10 Sv during ENSO cycle. Time sampling of our data set is clearly insufficient to infer interannual variability associated with ENSO; for indicative purposes only, ENSO phases are indicated on Fig. 11 by different colors of the year label (using the definition of the NOAA Climate Prediction Center).

5. Summary and conclusions

We used SADCP data from 94 cruises crossing the Solomon Sea and adjacent regions to describe the mean circulation and seasonal variability of the upper (20–100 m) and thermocline (100–300 m) layers in the Solomon Sea. A gridded monthly field of velocities with ¼° horizontal resolution was produced. The resulting circulation was compared to two independent velocity products inferred from hydrological data (CARS) and satellite and in situ data (CMDT CNES-CLS09).

This source of data provides an unprecedented description of the mean circulation in the Solomon Sea from in situ observations, and demonstrates how gathering even occasional SADCP historical data can be constructive. We show that the mean circulation is consistent with that previously described from sparse hydrological observations (Fine et al., 1994) and from a high-resolution model (Melet et al., 2010a). The SADCP analysis allows a detailed description of the complex western boundary current system pathways from direct observations of velocity. The NGCU enters the Solomon Sea east of Louisiade Archipelago, flows around the Woodlarks, splits against New Britain forming two branches that respectively flow westward and eastward. The two branches exit the Solomon Sea through Vitiaz Strait (around 7–8 Sv), St. George's Channel (1–2 Sv) and Solomon Strait (4–5 Sv) in the upper 300 m. In these three passages, the vertical structure of the currents shows velocity cores located around 150–300 m depth. The SADCP data also reveals weaker flow entering the Solomon Sea through two narrow passages, Jomard Entrance (about 0.3 Sv) and Indispensable Strait (about 1.2 Sv). In the surface layer, circulation patterns are similar except in the eastern part of the Solomon bain, where waters appear to enter the Solomon Sea from the northeast through Solomon Strait and exit either through the southern opening or through Vitiaz Strait.

High transport variability, primarily due to current magnitude modulation, is documented. At seasonal timescales, the LLWBCs, from the southern coast of the Louisiade Archipelago to north of Vitiaz Strait, strengthen in June–August, during the southeasterly monsoon. Distinctively, the boundary current exiting through Solomon Strait is stronger later in the year, in August–September–October. Mechanisms governing this seasonality remain to be understood.

High transport variability is also found within single seasons, with transports in some straits possibly doubling or even reversing from 1 cruise to another. For example, in Vitiaz Strait, the total transport in the 0–300 m layer varies from 3 Sv to 12 Sv. Whether this is interannual variability related to ENSO or intraseasonal variability related to the Madden–Julian Oscillation (Zhang, 2005) or due to local wind events is currently impossible to tell given the lack of continuous time series.

Our results are limited in several ways. First of all, our analyses were restricted to the upper 300 m, since only few cruises made deeper SADCP measurements. Observations from LADCP (Maes et al., 2009) and glider data (not shown) reveal that the core of the LLWBCs can be deeper, notably at the southern entrance of the Solomon Sea. Direct measurements of deeper current would therefore be very enlightening to fully describe the LLWBCs' structures. Nevertheless, the present database is able to pick up the core of the currents in the straits in the northern part of the Solomon Sea.

Secondly, our seasonal climatology and the seasonal variability inferred from the SADCP data (Fig. 10) is certainly biased in some regions by strong signals from interannual or intraseasonal events, unresolved by the available sampling. The only way to unambiguously resolve the various timescales of current variability at given locations would be to deploy moorings, as recommended by the CLIVAR/SPICE (Southwest PacIfic Ocean Circulation and climate Experiment) international research project (Ganachaud et al., 2007, 2008).

In this context, several moorings deployments in the straits are planned for the near future. Continuous time series of velocities in all straits would be of utmost importance. They would allow a full description of the different timescales of transport variability, resolve tidal ambiguities, corroborate (or not) the seasonal variability described here, and measure intraseasonal and interannual variability. They would also measure deep transports that may be important for the feeding of the equatorial current system below the thermocline.

Acknowledgments

This study has been possible thanks to the effort of many scientists, engineers and crews who carefully recorded, processed and made available SADCP data. The authors recognize the hard work done to accomplish this task, and are very grateful to all who contributed. SADCP data were downloaded freely from various databases. Many of them come from the Joint Archive for Shipboard ADCP (JASADCP, http://ilikai.soest.hawaii.edu/sadcp/main_inv.html). We greatly thank E. Firing, J. Hammon and P. Caldwell for maintaining this resource. Other SADCP data come from R/V Franklin (http://www.marine.csiro.au/maru/marlin_admin.survey_list), and from IRD (P. Grimigni, E. Kestenare, http://www.ird.nc/ECOP/sadcp_inventory.html). The authors also wish to thank M. Tivey, C. Maes and J. Murray who made their SADCP cruise available. The authors wish to thank Laurent Testut who kindly made the tidal analyses and hindcasts, and M.-H. Rio who provided the modified CMDT product, answered questions about it and made specific analyses very useful for this study. L. Gourdeau, A. Melet, T. Delcroix, E. Kestenare and an anonymous reviewer made useful comments about an earlier version of this manuscript. The authors finally wish to acknowledge use of the Ferret program for analysis and graphics in this paper. Ferret is a product of NOAA's Pacific Marine Environmental Laboratory. (Information is available at http://ferret.pmel.noaa.gov/Ferret.). This work is co-funded by ANR project ANR-09-BLAN-0233-01 and INSU/LEFE project IDAO; it is a contribution to the CLIVAR/SPICE International program (http://www.clivar.org; http://www.solomonseaoceanography.org). This is PMEL Contribution # 3563.

References

Burrage, D.M., 1993. Coral sea currents. Corella 17, 135–145.
Butt, J., Lindstrom, E., 1994. Currents off the east coast of New Ireland, Papua New Guinea, and their relevance to regional undercurrents in the western equatorial Pacific Ocean. Journal of Geophysical Research – Oceans 99 (C6).
Chang, P., Yamagata, T., Schopf, P., Behera, S.K., Carton, J., Kessler, W.S., Meyers, G., Qu, T., Schott, F., Shetye, S., Xie, S.P., 2006. Climate fluctuations of tropical coupled systems – the role of ocean dynamics. Journal of Climate 19 (20), 5122–5174.
Chen, S.M., Qiu, B., 2004. Seasonal variability of the South Equatorial Countercurrent. Journal of Geophysical Research – Oceans 109 (C8).
Condie, S.A., Dunn, J.R., 2006. Seasonal characteristics of the surface mixed layer in the Australasian region: implications for primary production regimes and biogeography. Marine and Freshwater Research 57 (6), 569–590.
Cresswell, G.R., 2000. Coastal currents of northern Papua New Guinea, and the Sepik River outflow. Marine and Freshwater Research 51 (6), 553–564.

De Mey, P., Ménard, Y., 1989. Synoptic analysis and dynamical adjustment of GEOS 3 and Seasat altimeter Eddy fields in the northwest Atlantic. Journal of Geophysical Research 94, 6221–6231.

Dutrieux, P., Firing, E., Hummon, J., Kashino, Y., Richards, K., Menkes, C., Sasaki, H., submitted for publication. Direct measurements of upper to intermediate ocean currents in the north-western tropical Pacific.

Fedorov, A.V., Philander, S.G., 2000. Is El Nino changing? Science 288 (5473), 1997–2002.

Fine, R.A., Lukas, R., Bingham, F.M., Warner, M.J., Gammon, R.H., 1994. The western equatorial Pacific – a water mass crossroads. Journal of Geophysical Research – Oceans 99 (C12), 25063–25080.

Fukumori, I., Lee, T., Cheng, B., Menemenlis, D., 2004. The origin, pathway, and destination of Nino-3 water estimated by a simulated passive tracer and its adjoint. Journal of Physical Oceanography 34 (3), 582–604.

Ganachaud, A., Kessler, W., Wijffels, S., Ridgway, K., Cai, W., Holbrook, N., Bowen, M., Sutton, P., Qiu, D., Timmermann, A., Roemmich, D., Sprintall, J., Cravatte, S., Gourdeau, L., Aung, T., 2007. Southwest Pacific Ocean Circulation and Climate Experiment (SPICE). Part I. Scientific Background. NOAA OAR Special Report, International CLIVAR Project Office, CLIVAR Publication Series No. 111, Journal (Issue).

Ganachaud, A., Brassington, G., Kessler, W., Mechoso, C.R., Wijffels, S., Ridgway, K., Cai, W., Holbrook, N., Sutton, P., Bowen, M., Qiu, B., Timmermann, A., Roemmich, D., Sprintall, J., Neelin, D., Lintner, B., Diamond, H., Cravatte, S., Gourdeau, L., Eastwood, P., Aung, T., 2008. Southwest Pacific Ocean Circulation and Climate Experiment (SPICE). Part II. Implementation Plan, NOAA OAR Special Report, International CLIVAR Project Office, CLIVAR Publication Series No. 133.

Giese, B.S., Urizar, S.C., Fuckar, N.S., 2002. Southern Hemisphere origins of the 1976 climate shift. Geophysical Research Letters 29 (2), 4.

Gordon, R.M., Coale, K.H., Johnson, K.S., 1997. Iron distribution in the equatorial Pacific: implications for new production. Limnology and Oceanography 43 (3), 419–431.

Gourdeau, L., 1998. Internal tides observed at 2°S, 156°E by in situ and TOPEX/POSEIDON data during the Coupled Ocean-Atmosphere Response Experiment (COARE). Journal of Geophysical Research 103 (C6), 12629.

Gu, D.F., Philander, S.G.H., 1997. Interdecadal climate fluctuations that depend on exchanges between the tropics and extratropics. Science 275 (5301), 805–807.

Hazeleger, W., Seager, R., Cane, M.A., Naik, N.H., 2004. How can tropical Pacific Ocean heat transport vary? Journal of Physical Oceanography 34 (1), 320–333.

Hummon, J., Firing, E., 2003a. Notes from Acoustic Doppler Current Profiler Workshop at the National Oceanographic Data Center, May 14–15, 1992.

Hummon, J.M., Firing, E., 2003b. A direct comparison of two RDI shipboard ADCPs: a 75-kHz ocean surveyor and a 150-kHz narrow band. Journal of Atmospheric and Oceanic Technology 20 (6), 872–888.

Ishida, A., Kashino, Y., Hosoda, S., Ando, K., 2008. North-south asymmetry of warm water volume transport related with El Nino variability. Geophysical Research Letters 35 (18).

Izumo, T., 2005. The equatorial undercurrent, meridional overturning circulation, and their roles in mass and heat exchanges during El Nino events in the tropical Pacific ocean. Ocean Dynamics 55, 110–123.

Johnson, G.C., McPhaden, M.J., 1999. Interior pycnocline flow from the subtropical to the equatorial Pacific Ocean. Journal of Physical Oceanography 29 (12), 3073–3089.

Johnson, G.C., Sloyan, B.M., Kessler, W.S., McTaggart, K.E., 2002. Direct measurements of upper ocean currents and water properties across the tropical Pacific during the 1990s. Progress in Oceanography 52 (1), 31–61.

Kashino, Y., Ueki, I., Kuroda, Y., Purwandani, A., 2007. Ocean variability north of New Guinea derived from TRITON buoy data. Journal of Oceanography 63 (4), 545–559.

Kessler, W.S., Gourdeau, L., 2007. The annual cycle of circulation of the southwest subtropical pacific, analyzed in an ocean GCM. Journal of Physical Oceanography 37 (6), 1610–1627.

Kleeman, R., McCreary, J.P., Klinger, B.A., 1999. A mechanism for generating ENSO decadal variability. Geophysical Research Letters 26 (12), 1743–1746.

Kuroda, Y., 2000. Variability of currents off the northern coast of New Guinea. Journal of Oceanography 56 (1), 103–116.

Lee, T., Fukumori, I., 2003. Interannual-to-decadal variations of tropical–subtropical exchange in the Pacific Ocean: boundary versus interior pycnocline transports. Journal of Climate 16 (24), 4022–4042.

Lindstrom, E., Lukas, R., Fine, R., Firing, E., Godfrey, S., Meyers, G., Tsuchiya, M., 1987. The western equatorial Pacific Ocean circulation study. Nature 330 (6148), 533–537.

Lindstrom, E., Butt, J., Lukas, R., Godfrey, S., 1990. The flow through Vitiaz Strait and St. George's Channel, Papua New Guinea. The Physical Oceanography of Sea Straits, 171–189.

Lohmann, K., Latif, M., 2005. Tropical Pacific decadal variability and the subtropical–tropical cells. Journal of Climate 18 (23), 5163–5178.

Lübbecke, J.F., Böning, C.W., Biastoch, A., 2008. Variability in the subtropical–tropical cells and its effect on near-surface temperature of the equatorial Pacific: a model study. Ocean Science 4 (1), 73–88.

Lukas, R., Yamagata, T., McCreary, J.P., 1996. Pacific low-latitude western boundary currents and the Indonesian throughflow. Journal of Geophysical Research – Oceans 101 (C5), 12209–12216.

Lumpkin, R., Garraffo, Z., 2005. Evaluating the decomposition of tropical Atlantic drifter observations. Journal of Atmospheric and Oceanic Technology 22, 1403–1415.

Lumpkin, R., Pazos, M., 2006. Measuring surface currents with Surface Velocity Program drifters: the instrument, its data, and some recent results. In: Griffa, A., Kirwan, A.D., Mariano, A.J., Ozgokmen, T., Rossby, T. (Eds), Chapter Two of Lagrangian Analysis and Prediction of Coastal and Ocean Dynamics (LAPCOD).

Luo, Y.Y., Rothstein, L.M., Zhang, R.H., Busalacchi, A.J., 2005. On the connection between South Pacific subtropical spiciness anomalies and decadal equatorial variability in an ocean general circulation model. Journal of Geophysical Research – Oceans 110 (C10).

Lyard, F., Le Provost, C., 2002 Energy budget of the tidal hydrodynamic model fes99. Appears in C. LeProvosts' talk: ocean tides after a decade of high precision satellite altimetry", SWT Jason 1, Arles, 2003.

Lyard, F. et al., 2006. Modelling the global ocean tides: modern insights from FES2004. Ocean Dynamics 56 (5–6), 394–415.

Mackey, D.J., O'Sullivan, J.E., Watson, R.J., 2002. Iron in the western Pacific: a riverine or hydrothermal source for iron in the Equatorial Undercurrent? Deep-Sea Research Part I – Oceanographic Research Papers 49, 877–893.

Maes, C., Eldin, G., Melet, A., Lefévre, J., Sudre, J., Varillon, D., Ganachaud, A., Gourdeau, L., 2009. Rapport de la mission océanographique FLUSEC-01 à bord du N. O. Alis du 12 au 30 Août 2007 en mer de Corail, Océan Pacifique Sud-Ouest, Rapports de missions, Sciences de la Mer, Océanographie Physique, Centre IRD de Nouméa, Nouvelle Calédonie, No. 24, 98 pp.

Matei, D., Keenlyside, N., Latif, M., Jungclaus, J., 2008. Subtropical forcing of tropical Pacific climate and decadal ENSO modulation. Journal of Climate 21 (18), 4691–4709.

McCreary, J.P., Lu, P., 1994. Interaction between the subtropical and equatorial ocean circulations: the subtropical cell. Journal of Physical Oceanography 24 (2), 466–497.

McPhaden, M.J., Zhang, D.X., 2002. Slowdown of the meridional overturning circulation in the upper Pacific Ocean. Nature 415 (6872), 603–608.

Melet, A., 2010. Les circulations océaniques en mer des Salomon: modélisation haute-résolution et altimetry spatiale, these de doctorat de l'Université Joseph Fourier, Grenoble, p. 235.

Melet, A., Gourdeau, L., Kessler, W.S., Verron, J., Molines, J.M., 2010a. Thermocline circulation in the Solomon Sea: a modeling study. Journal of Physical Oceanography 40, 1302–1319.

Melet, A., Gourdeau, L., Verron, J., 2010b. Variability in Solomon Sea circulation derived from altimeter sea level data. Ocean Dynamics 60, 883–900.

Murray, S., Lindstrom, E., Kindle, J., Weeks, E., 1995. Transport through the Vitiaz Strait. WOCE Notes 7 (1), 21–23.

Nonaka, M., Xie, S.P., McCreary, J.P., 2002. Decadal variations in the subtropical cells and equatorial Pacific SST. Geophysical Research Letters 29 (7), 20–31.

Qiu, B., Chen, S., Kessler, W.S., 2009. Source of the 70-day mesoscale eddy variability in the Coral Sea and the North Fiji Basin. Journal of Physical Oceanography 39, 404–420.

Qu, T.D., Lindstrom, E.J., 2002. A climatological interpretation of the circulation in the Western South Pacific. Journal of Physical Oceanography 32 (9), 2492–2508.

Ridgway, K.R., Godfrey, J.S., Meyers, G., Bailey, R., 1993. Sea Level Response to the 1986–1987 El-Nino Southern Oscillation event in the Western Pacific in the Vicinity of Papua New Guinea. Journal of Geophysical Research – Oceans 98 (C9), 16387–16395.

Ridgway, K.R., Dunn, J.R., Wilkin, J.L., 2002. Ocean interpolation by four-dimensional weighted least squares – application to the waters around Australasia. Journal of Atmospheric and Oceanic Technology 19 (9), 1357–1375.

Rio, M.H., Hernandez, F., 2004. A mean dynamic topography computed over the world ocean from altimetry, in situ measurements, and a geoid model. Journal of Geophysical Research – Oceans 109 (C12), C12032.

Rio, M.H., Schaeffer, P., Moreaux, G., Lemoine, J.M., Bronner, E., 2009. A new Mean Dynamic Topography Computed over the Global Ocean from GRACE Data, Altimetry and In-situ Measurements. Poster Communication at OceanObs09 Symposium, 21–25 September, 2009, Venice.

Schott, F.A., McCreary, J.P., Johnson, G.C., 2004. Shallow overturning circulations of the tropical–subtropical oceans. In: Earth Climate: The Ocean Atmosphere Interaction, Geophysical Monograph, vol. 147, p. 261304.

Schott, F.A., Wang, W.Q., Stammer, D., 2007. Variability of Pacific subtropical cells in the 50-year ECCO assimilation. Geophysical Research Letters 34 (5).

Slemons, L.O., Murray, J.W., Resing, J., Paul, B., Dutrieux, P., 2010. Western Pacific coastal sources of iron, manganese, and aluminum to the Equatorial Undercurrent, Global Biogeochemical Cycles 24, 16.

Sokolov, S., Rintoul, S., 2000. Circulation and water masses of the southwest Pacific: WOCE section P11, Papua New Guinea to Tasmania. Journal of Marine Research 58, 223–268.

Sun, D.Z., Zhang, T., Shin, S.I., 2004. The effect of subtropical cooling on the amplitude of ENSO: a numerical study. Journal of Climate 17 (19), 3786–3798.

Tsuchiya, M., 1968. Upper Waters of the Intertropical Pacific Ocean, Johns Hopkins Oceanogr. Stud., No. 4, 50 pp.

Tsuchiya, M., 1981. The origin of the Pacific equatorial 13C water. Journal of Physical Oceanography 11 (6), 794–812.

Tsuchiya, M., Lukas, R., Fine, R.A., Firing, E., Lindstrom, E., 1989. Source waters of the Pacific Equatorial Undercurrent. Progress in Oceanography 23 (2), 101–147.

Ueki, I., Kashino, Y., Kuroda, Y., 2003. Observation of current variations off the New Guinea coast including the 1997–1998 El Nino period and their relationship with Sverdrup transport. Journal of Geophysical Research – Oceans 108 (C7).

Yeager, S.G., Large, W.G., 2004. Late-winter generation of spiciness on subducted isopycnals. Journal of Physical Oceanography 34 (7), 1528–1547.

Zenk, W., Siedler, G., Ishida, A., Holfort, J., Kashino, Y., Kuroda, Y., Miyama, T., Müller, T.J., 2005. Pathways and variability of the Antarctic Intermediate Water in the western equatorial Pacific Ocean. Progress in Oceanography 67, 245–281.

Zhang, C.D., 2005. Madden–Julian oscillation. Reviews of Geophysics 43 (2).